Applied Catalysis B: Environmental 144 (2014) 665–673

Contents lists available at ScienceDirect

Applied Catalysis B: Environmental

journal homepage: www.elsevier.com/locate/apcatb

Distinctive polypyrrole nanobelts as prospective electrode for the direct detection of aliphatic alcohols: Electrocatalytic properties

Sadia Ameen[a,1], M. Shaheer Akhtar[b,1], Hyung-Kee Seo[a], Hyung Shik Shin[a,*]

[a] Energy Materials & Surface Science Laboratory, Solar Energy Research Center, School of Chemical Engineering, Chonbuk National University, Jeonju 561-756, Republic of Korea
[b] New & Renewable Energy Material Development Center (NewREC), Chonbuk National University, Jeonbuk, Republic of Korea

ARTICLE INFO

Article history:
Received 26 April 2013
Received in revised form 25 June 2013
Accepted 24 July 2013
Available online 6 August 2013

Keywords:
Polypyrrole
Aliphatic alcohols
Chemical sensor
Sensitivity
Electrochemical impedance spectroscopy

ABSTRACT

The effective working electrode based on polypyrrole (PPy) nanobelts was employed for the fabrication of highly sensitive and reproducible aliphatic alcohols chemical sensor. The unique PPy nanobelts were simply synthesized by in situ chemical polymerization of pyrrole monomer in the presence of ferric chloride as oxidant and methylene blue as reactive self-degraded template. The morphological properties and elemental mapping revealed that the synthesized PPy nanobelts possessed the uniform dimension with high aspect of chemical compositions. The PPy nanobelts electrode showed reasonably high electrical conductivity of ~1.80×10^{-4} Ω^{-1} cm^{-1}. The electrochemical and electrocatalytic behavior of PPy nanobelts based electrode toward the detection of aliphatic alcohols were elucidated by measuring the electrochemical impedance spectroscopy (EIS) measurements. Furthermore, the current (I)–voltage (V) characteristics were performed to evaluate the sensing performance of PPy nanobelts electrode toward the detection of aliphatic alcohols. Among different aliphatic alcohols, the methanol chemical sensor based on PPy nanobelts electrode displayed the highest sensitivity of ~205.64 μA mM^{-1} cm^{-2}, good detection limit of ~6.92 μM with correlation coefficient (R) of ~0.98271 and short response time (10 s).

1. Introduction

The major environment pollutants like CO_2, CO, SO_2 and volatile organic compounds (VOCs) are usually produced by the consumption of commonly used chemicals such as ammonia (NH_3), ethanol (C_2H_5OH), methanol (CH_3OH) and other aliphatic alcohols [1]. Moreover, the excessive use of VOCs such as aliphatic alcohols and ketones are continuously polluting the environment and causes the health problems [2]. Methanol is highly used as automotive fuel in motor vehicles and in making dyes and perfumes [3]. The surplus exposure of methanol to human could cause blindness, metabolic acidosis and might lead to death [4]. The combustion of other alcohol like propanol releases the toxic materials which are harmful to human beings [5]. The sensor technology is well known tool for the detection of VOCs such as, alcohols, ethers, esters, halocarbons, ammonia, NO_2 and warfare agent stimulants [6] and is highly demanding in industries, medicines and for domestic applications to detect the pollutants, toxic and harmful chemicals [7]. The electrochemical sensors have received much attention as promising chemical sensing tool to detect the harmful chemicals [8]. In this regards, the designing of effective working electrode with high electron transfer rate is still a challenge. The chemical sensor based on working electrodes of different nanomaterials such as polymers and metal oxide semiconductors are promising for the reliable detection of harmful chemicals owing to their reliability, high surface-to-bulk ratio, good adsorption characteristics and high selectivity [9].

Conjugated polymers are known as p-type semiconductors with unique electronic properties due to their reasonable electrical conductivity, low energy optical transitions, low ionization potential and high electron affinity [10]. These polymers could be easily synthesized through simple chemical or electrochemical processes and their conductivities could be altered by modifying the electronic structures through doping or de-doping procedures [11]. Therefore, conducting polymers could suitably work as an effective working electrode and might offer the fast response toward the detection of various harmful chemicals [7]. In general, the good selectivity, wide linear range, rapid response, portability and the room temperature working abilities are the basic requirements for the efficient working of chemical sensors [12]. Polypyrrole (PPy), a conducting polymer, is much explored material because it shows high electrical conductivity, high stability in air and aqueous media and thus, an extremely useful material for actuators, electric devices and for the efficient detection of the harmful chemicals [13,14]. Few literatures are reported on the sensor performances of

* Corresponding author. Fax: +82 63 270 2306.
E-mail address: hsshin@jbnu.ac.kr (H.S. Shin).
[1] [1]Authors contributed equally to this work.

0926-3373/$ – see front matter © 2013 Elsevier B.V. All rights reserved.
http://dx.doi.org/10.1016/j.apcatb.2013.07.053

PPy nanostructure based electrodes for the detection of aliphatic alcohols S. J. Hong et al. studied nitro vinyl substituted PPy as a unique reaction-based chemosensor for cyanide anion [15]. Lin et al. prepared the composite electrode of PPy-poly vinyl alcohol (PVA) by electrochemical method for the detection of methanol and ethanol vapor [16,17]. Jiang et al. prepared the composite films of PPy–PVA by in situ vapor state polymerization method and demonstrated the methanol sensing behavior based on the thickness of PPy–PVA film electrodes [18]. Recently, Babaei et al. determined the residual methanol content in the biodiesel samples by developing new PPy–ClO_4 electrodes via electrodeposition on interdigital electrodes [19]. The roughness and morphology of the PPy greatly influence the responses for the detection of harmful chemicals [20]. In this context, the unique and effective working electrode based on PPy nanobelts has been utilized for the fabrication of highly sensitive and reproducible aliphatic alcohols chemical sensor. The unique PPy nanobelts are simply synthesized by the in situ chemical polymerization of pyrrole monomer in presence of ferric chloride as oxidant and methylene blue as reactive self-degraded template. To the best of our knowledge, for the first time, PPy nanobelts have been directly applied as working electrode for the efficient detection of aliphatic alcohols using simple current (I)–voltage (V) characteristics.

2. Experimental

2.1. Synthesis of PPy nanobelts

In a typical synthesis of PPy nanobelts, 20.0 mmol of PPy monomer (1.4 ml, Sigma–Aldrich, ≥99.5%) and 4.0 mmol of methylene blue (1.27 g) were mixed in 30 ml DI (deionized) water under vigorous stirring for 30 min. Thereafter, 1 M (33.4 ml) dopant solution of ferric chloride ($FeCl_3$, Daejung, ≥99.5%) was added dropwise into the reactant mixture and the reaction was kept for 20 h under static condition at 5 °C. The obtained precipitates were centrifuged at ~4500 rpm for 10 min and the products were washed with copious amount of DI water, methanol and dried in vacuum oven. Herein, methylene blue played a significant role to obtain the morphology of nanobelts. The methylene blue generally has a planar hydrophobic section and hydrophilic end group and thus, acts as anionic template in aqueous solution. However, the methylene blue in aqueous acidic solution could dimerize and produce the oligomers which finally degrade during the polymerization, resulting to the formation of PPy nanobelts with the high surface area of ~46.6 m^2/g [21,22].

2.2. Characterization of PPy nanobelts

The morphological observations were studied by using field emission scanning electron microscopy (FESEM, Hitachi S-4700, Japan), transmission electron microscopy (TEM, JEM-2010-JEOL, Japan) and the atomic force spectroscopy (AFM, Nanoscope IV, Digital Instruments, Santa Barbara, USA). The line scan element mapping was analyzed by the FESEM coupled Energy dispersive X-ray spectroscopy with the mapping mode. Raman spectra (Raman microscope, Renishaw) and Fourier transform infrared spectra (FTIR, Nicolet, IR300) were used for the structural characterizations. The ^{1}H NMR spectra of PPy nanobelts electrode in DMSO solvent were recorded by 600 MHz FT-NMR spectrometer (JNM-ECA600). The optical properties were characterized by the photoluminescence studies (JASCO, FP-6500) and UV–visible absorbance (2550 Shimadzu, Japan). The electrochemical impedance spectroscopy (EIS) measurements were carried out by VersaSTAT4 by using the two probes electrochemical system. PPy nanobelts electrode was used as working and Pt wire electrode as cathode in PBS solution of different concentrations of aliphatic alcohols under the ac signal of 5 mV over the frequency range of 100 kHz–1 Hz.

2.3. Fabrication and characterization of PPy nanobelts based aliphatic alcohol chemical sensor

Bulk samples in the form of pellets were prepared by compressing the finely grounded PPy nanobelts powder under a pressure of ~6.6 Ton. The prepared PPy electrode shows the surface area of ~39.8 m^2/g. The contacts were made by attaching the thin Cu wire on the pellet through the silver paste. Thereafter, the electrode was subjected to drying at 60 ± 5 °C for 2 h in an electric oven. The sensing performances of aliphatic alcohols were studied by a simple two electrode I–V characteristics using PPy nanobelts electrode as working and Pt wire as a cathode. The I–V characteristics were measured by the electrometer (Keithley, 6517A, USA). A fixed amount of 0.1 M phosphate buffer solution (PBS, 10.0 ml) of pH 7 and the wide concentration range of aliphatic alcohols (methanol, propanol and butanol) from 20 μM–1 mM were used for the experiments. The sensitivity of the fabricated alcohol chemical sensor was estimated by the slope of the current vs. concentration from the calibration plot, divided by the value of active area of sensor/electrode. The current response was measured from 0–2.5 V and the response time was measured as 10 s.

3. Results and discussion

3.1. Morphological characterizations of PPy nanobelts

The morphology of the synthesized PPy nanomaterials is analyzed by FESEM and TEM images, as shown in Fig. 1. From FESEM images (Fig. 1(a) and (b)), the synthesized PPy nanomaterials possess smooth and the uniform belt like morphology. Each PPy nanobelt presents the average thickness of ~100 nm and width of ~400 nm, as shown in Fig. 1(b). The morphology of the synthesized PPy has been further characterized by the TEM analysis (Fig. 1(c)). Similar morphology and the dimensions are observed in TEM image, which is consistent with the FESEM results. Interestingly, the morphology of PPy nanobelts has not changed under high energy electron beam, indicating the stability of PPy nanobelts.

Fig. 2 shows the topographic and three dimensional (3D) AFM images of synthesized PPy nanobelts. As observed in FESEM and TEM analysis, the nanobelts morphology is visibly seen in the AFM images. The synthesized PPy nanobelts show the reasonable root mean roughness (R_{ms}) of ~18.1 nm. It is reported that the high electrochemical behavior and electrocatalytic activity of electrode are related to the large roughness factor of the electrode materials [23]. In our case, the PPy nanobelts with reasonable R_{ms} value might deliver the electrochemical behavior toward the detection of aliphatic alcohols.

The elemental compositions of the synthesized PPy nanobelts are estimated by the element line scan image through EDS, as depicted in Fig. 3. The line scan image and pie profile (Fig. 3(a) and (b)) display that the synthesized PPy nanobelts are largely composed of carbon and nitrogen elements. Few traces of oxygen elements are also recorded which might due to surface moisture or atmospheric oxygen on the surface of nanobelts. Fig. 3(c) summarizes the existing elements of PPy nanobelts in weight percentage (wt%) and atomic percentage (at%). The synthesized PPy nanobelts are consisted of uniformly distributed carbon and nitrogen with at% of ~60.09 and ~39.41 respectively. The detection of C, N and O elements confirm the formation of synthesized PPy nanobelts.

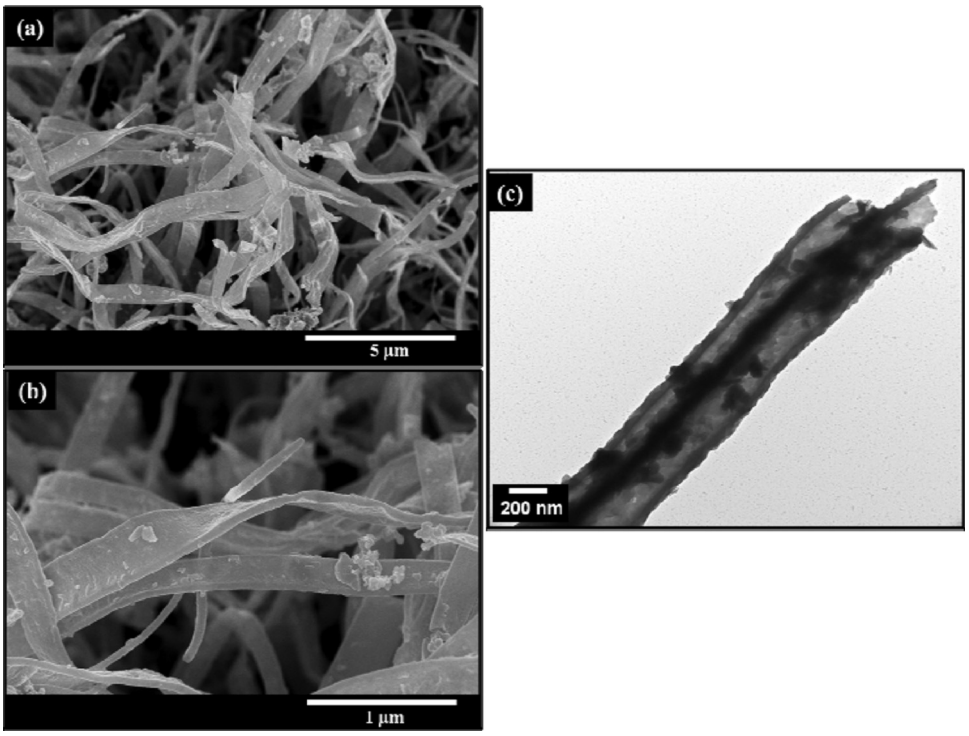

Fig. 1. FESEM images at (a) low and (b) high resolution and (c) TEM image of PPy nanobelts.

3.2. Structural and optical characterizations of PPy nanobelts

FTIR spectroscopy analysis of synthesized PPy nanobelts is examined to elucidate the structures of PPy, as shown in Fig. 4. The IR peaks at ~1553 and ~1483 cm^{-1} present the characteristic peaks of PPy, corresponding to the C=C antisymmetric and symmetric stretching vibration in PPy ring respectively [24]. The IR peaks at ~1308 cm^{-1} and ~1204 cm^{-1} are ascribed to C—N stretching vibration and the C—C stretching in PPy nanobelts [25]. The appearance of two IR peaks at ~1192 and ~798 cm^{-1} are assigned to C—C stretching of PPy backbone. Additionally, the C—H deformation and C—H rocking vibration are confirmed by the appearance of IR peaks at ~924 cm^{-1} and ~651 cm^{-1} respectively [26]. A broad IR peak at ~3224 cm^{-1} and small peak at ~1958 cm^{-1} are attributed to N—H stretching and the stretching vibration of the CN group in PPy nanobelts respectively [27,28].

The Raman scattering spectroscopy has been used to analyze the structural properties of PPy nanobelts. Fig. 5(a) shows the Raman spectrum of synthesized PPy nanobelts. The strong Raman band at ~1558 cm^{-1} corresponds to the characteristics C=C backbone stretching of PPy [29]. The Raman bands at ~1317 cm^{-1} and ~1044 cm^{-1} are attributed to the ring-stretching mode and the C—H in-plane of PPy respectively [30]. However, the peaks at ~972 cm^{-1} confirms the ring deformation, associated with the

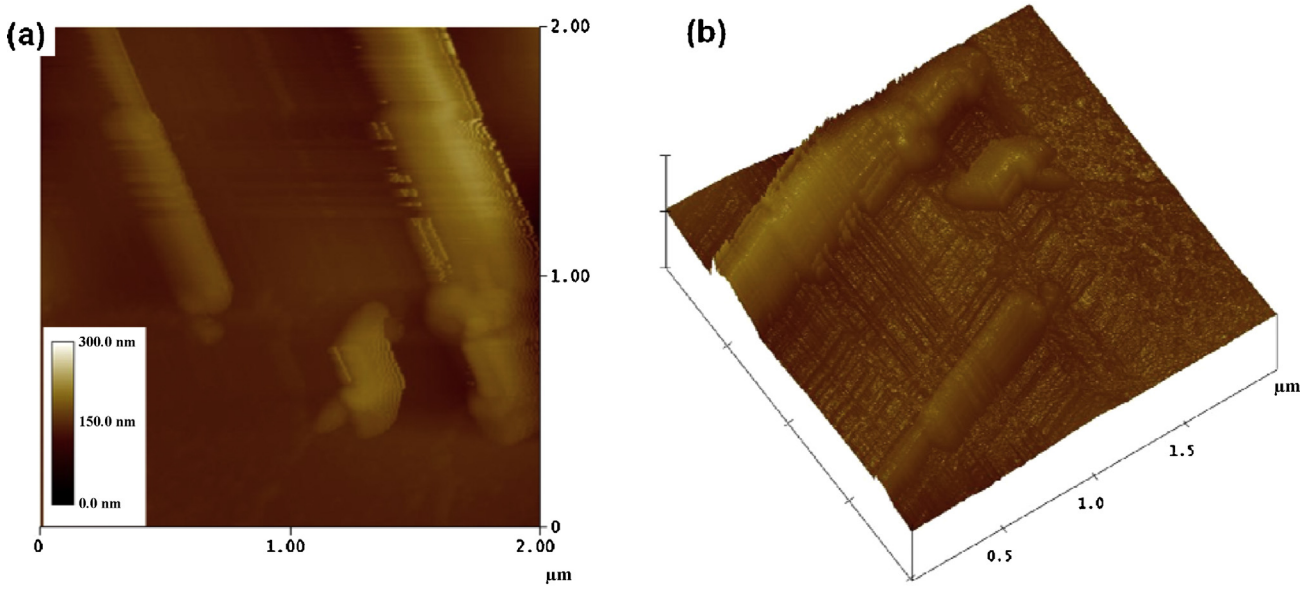

Fig. 2. (a) Topographic and (b) three dimensional AFM images of PPy nanobelts.

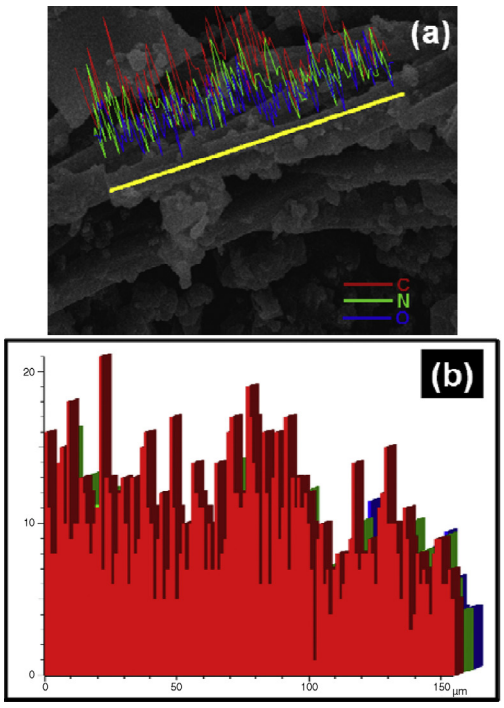

(c)

Element	Weight (%)	Atomic (%)
C	58.03	60.09
N	40.11	39.41
O	1.85	0.50
Total	100	

Fig. 3. (a) Line scanning elemental mapping image, (b) corresponding pie bar graph and (c) summary of elemental mapping of PPy nanobelts.

radical cation (polaron) in PPy [31]. The detailed structure of PPy nanobelts are analyzed by the Raman mapping. The corresponding Raman mapping images in the two ranges of ~950–1050 cm^{-1} and ~1550–1600 cm^{-1} are depicted in Fig. 5(b) and (c). In the Raman mapping, the uniform scattered light green color in the major dark green area is seen in the range of 950–1050 cm^{-1} (Fig. 5(b)), which is assigned to the ring deformation associated with the radical cation (polaron) in PPy (Raman shift at ~972 cm^{-1}). (For interpretation of the references to color in the text, the reader is referred to the web version of the article.) On the other hand, the Raman mapping in the range of 1550–1600 cm^{-1} exhibits the uniform distribution of C=C stretching in PPy nanobelts, as shown in Fig. 5(c). Thus, the uniformly distributed C=C bonding along with ring deformation, associated with the radical cation (polaron) in Raman mapping confirms the formation of high quality of PPy nanobelts. These results are in excellent agreement with the FTIR results.

Fig. 6(a) exhibits the UV–Vis absorption spectrum of PPy nanobelts. The absorption band at ~277 nm is attributed to π–π^* transition in PPy nanobelts [32]. Another broad absorption band at ~521 nm presents the characteristic of an oxidized PPy [32]. The UV–Vis spectrum of PPy is similar to the reported literature [33]. The room temperature photoluminescence (PL) spectrum of PPy nanobelts is shown in Fig. 6(b) which is obtained with an excitation wavelength of ~360 nm. A single broad band in the blue-green region at ~448 nm is observed, corresponding to the non radiative quenching in the aggregated phase which might improve the charge carrier diffusion through the extended PPy chains [34]. Additionally, the generation of singlet excitons with the highest intensity might represent the arrangements of PPy nanoparticles in nanobelt morphology.

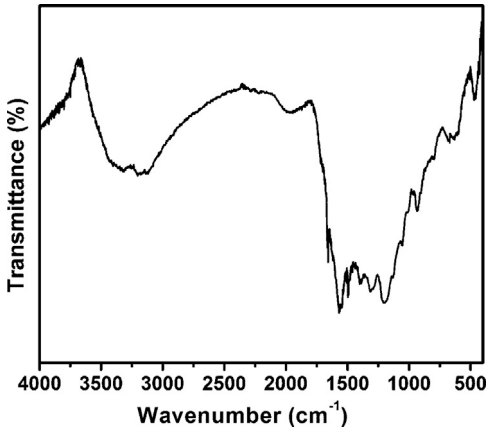

Fig. 4. FTIR spectrum of PPy nanobelts.

3.3. Aliphatic alcohol chemical sensor based on PPy nanobelts electrode

The electrochemical impedance spectroscopy (EIS) measurements have been performed for the fabricated aliphatic alcohols chemical sensors based on novel PPy nanobelts electrode to explain the electrocatalytic activity of the electrodes. Fig. 7 shows the EIS plots of the fabricated aliphatic alcohols chemical sensors based on novel PPy nanobelts electrode using 0.1 M phosphate sulfate solution (PBS) with methanol, propanol and butanol at similar concentration of 20 μM. All EIS measurements are carried out at a frequency range from 100 kHz–1 Hz. From Fig. 7, the fabricated aliphatic alcohols chemical sensor displays two semicircles, in which the large semicircle in the high frequency region is attributed to the parallel combination of the charge transfer resistance (R_{CT}) of the electrochemical reaction and the double layer capacitance (C_{dl}) at the interface of the PPy electrode/PBS electrolyte [35]. R_{CT} of sensor device defines the electron-transfer kinetics of the redox probe at the electrode interface [35]. In general, the signal response for sensing device is determined by the values of R_{CT} at the interfaces of the PPy electrode and different concentrations of alcohol in PBS [36]. Herein, all electrochemical alcohol chemical sensors present similar nature of EIS plots in 10 ml of PBS (0.1 M) with different alcohols at the same concentration of 20 μM. A relatively low R_{CT} value (~353 Ω) is obtained by the fabricated

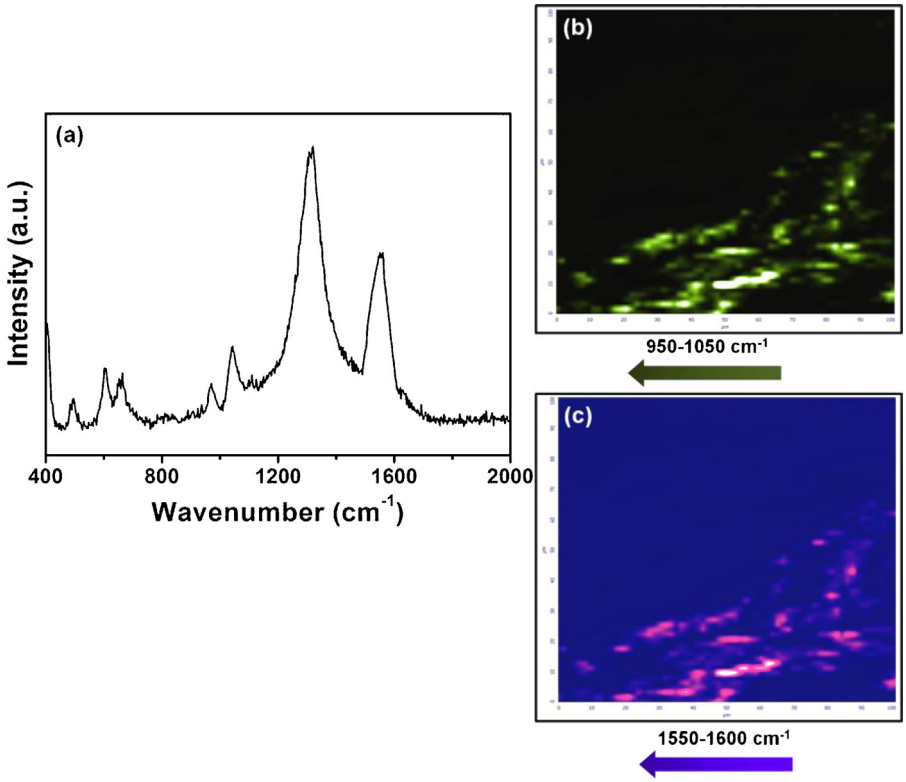

Fig. 5. (a) Raman spectrum and (b) corresponding Raman mapping images in 950–1050 cm^{-1} and (c) 1550–1600 cm^{-1} of PPy nanobelts.

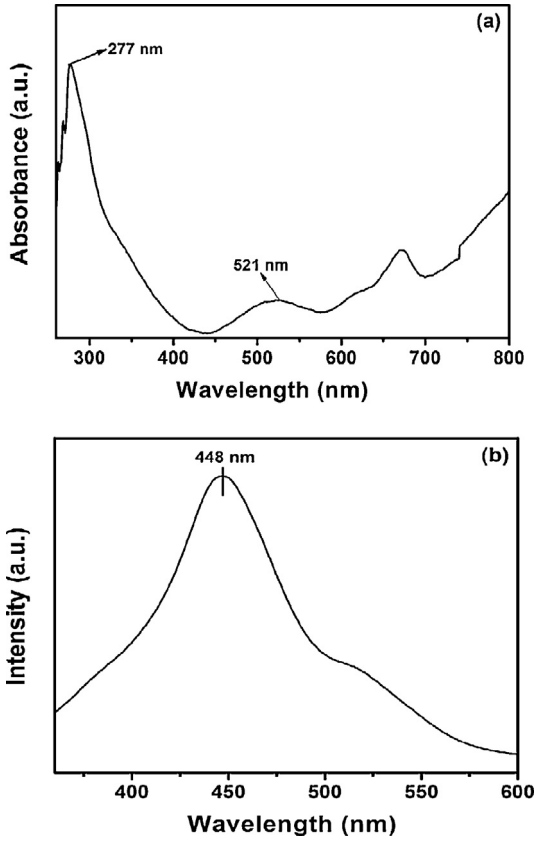

Fig. 6. (a) UV–vis and (b) PL spectrum of PPy nanobelts.

methanol chemical sensor based on PPy nanobelts electrode, however the propanol and butanol chemical sensors show the high R_{CT} values of ~507 Ω and ~597 Ω respectively. Generally, the low charge transfer rate at the interface of electrode/electrolyte in the electrochemical system is originated from high R_{CT} value [37]. This result suggests that the fabricated methanol chemical sensor based on PPy nanobelts electrode presents the better charge transfer rate and the electrocatalytic activity toward the methanol chemical, resulting to the high sensing response on the surface of PPy nanobelts electrode. Whereas, other aliphatic alcohols based chemical sensors are quite inferior to methanol chemical sensor.

Additionally, Fig. 8 shows the plots of $\ln\sigma_{dc}$ vs. $1000/T$ in the temperature range of 300 – 400 K for the prepared PPy nanobelts electrode. A reasonable high electrical conductivity of $\sim 1.80 \times 10^{-4}\ \Omega^{-1}\ cm^{-1}$ is recorded by the prepared PPy nanobelts

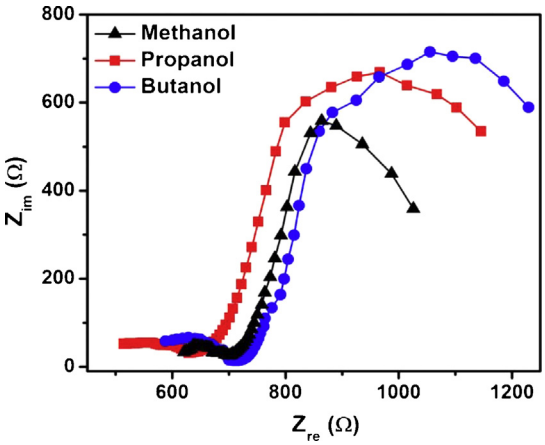

Fig. 7. EIS plots of fabricated different aliphatic alcohol sensors based on PPy nanobelts electrode.

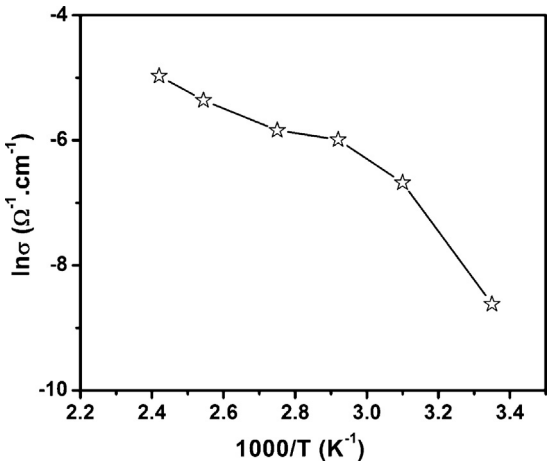

Fig. 8. Plots of DC conductivity vs 1000/*T* for PPy nanobelts based electrode.

electrode at room temperature (298 K). The electrical conductivity gradually increases with the increase of temperature from 298 to 423 K, indicating the stability and the maintained conductivity at high temperature. The reason of enhanced conductivity might arise due to the increased charged carrier concentration with the improved mobility of the charged carriers [38]. Like EIS results, the prepared PPy nanobelts electrode with high electrical conductivity might show high ions transport or charge transfer in the electrochemical system or sensors. Thus, the unique morphology of PPy nanobelt and methanol chemical significantly favor the high ions transport or charge transfer at the interface of PPy electrode and PBS.

The detailed sensing properties including the detection limit, linearity, correlation coefficient and sensitivity are extensively evaluated by the two electrodes *I–V* characteristics measurements where PPy nanobelts electrodes are used as working electrode while the Pt wire is applied as cathode. All *I–V* characteristics are measured with the applied voltage ranging from 0–2.5 V. The typical fabricated alcohol chemical sensor depicts the aliphatic alcohol sensing mechanism over the surface of PPy nanobelts. The fabricated aliphatic alcohol chemical sensor is performed in PBS with and without alcohols and the sensing behavior is simply explained by the *I–V* characteristics. It is noticed that the drastic increase in current is observed after the addition of aliphatic alcohols (20 μM) in all the fabricated chemical sensors as compared to chemical sensor without alcohol, as shown in inset of Fig. 9. The addition of methanol chemical (20 μM) in PBS displays the highest current of ~60.4 μA while the lower currents of ~58.7 μA and ~55.4 μA are obtained with the addition of propanol and butanol chemicals in PBS respectively. This gradual increase in the current indicates the rapid sensing response of PPy nanobelts electrode toward the detection of methanol, propanol and butanol chemicals, which might result from the better electrocatalytic or electrochemical behavior and the fast electron exchange of PPy nanobelts electrode. The *I–V* responses of PPy nanobelts electrode with various concentrations of aliphatic alcohols ranging from 20 μM–1 mM in 10 ml of 0.1 M PBS have been measured to investigate the detailed sensing behavior of PPy nanobelt electrode. Fig. 9(a) shows the *I–V* characteristics of the fabricated methanol chemical sensor with various concentrations of methanol chemical (20 μM–1 mM) in 0.1 M PBS solution of pH 7. When PPy nanobelts based electrode is exposed to methanol, the current drastically increases with the increase of the methanol concentrations, showing the good sensing response to methanol chemical. From the typical calibration curve (Fig. 9(b)), the fabricated methanol chemical sensor based on PPy nanobelts electrode exhibits the reproducible, reliable and the highest sensitivity of ~205.64 μA mM^{-1} cm^{-2} with the linearity of 20 μM–0.16 mM, detection limit of ~6.92 μM and correlation coefficient (*R*) of ~0.98271. However, the fabricated propanol and butanol chemical sensors based on PPy nanobelts electrode (Figs. 10 and 11) show the low sensitivities of ~190.76 and ~146.34 μA mM^{-1} cm^{-2} and moderate detection limits of ~13.7 and ~12.06 μM respectively. All aliphatic alcohol sensors display the same response time of 10 s. The sensing parameters of all sensors are summarized in Table 1. As compared to other aliphatic alcohols, the highest current response and sensitivity have been observed for methanol chemical sensing which might suggest the high electron mobility and electrochemical activity over the surface of PPy nanobelts electrode, as described in EIS results.

Fig. 12 depicts the schematic illustration of the proposed mechanism of aliphatic alcohol chemical sensors over the surface of PPy nanobelts electrode. The detection of aliphatic alcohol chemicals in liquid phase is generally obtained by the adsorption of oxygenated species in PBS to the surface of PPy nanobelts electrode. These adsorbed oxygenated species change the concentration of oxygen species due to surface reactions and thus, develops a potential barrier and enhances the resistance of the material [39] Further, the chemisorbed oxygen reacts with alcohols over the PPy nanobelts

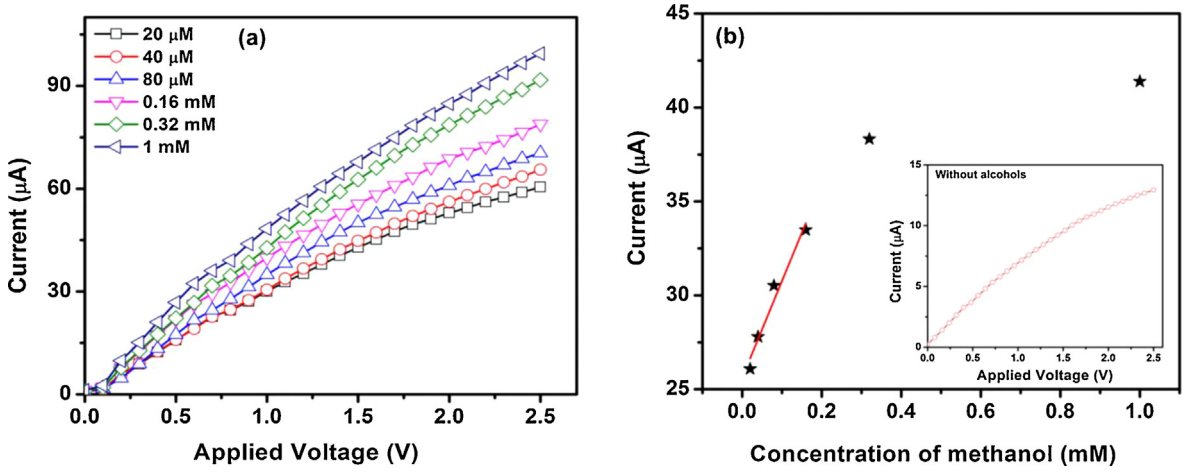

Fig. 9. (a) The *I–V* characteristics of PPy nanobelts based methanol chemical sensor at different methanol concentrations (20 μM–1 mM) in 10 ml of 0.1 M PBS and (b) the calibration curve of current versus methanol concentration of the fabricated chemical sensor.

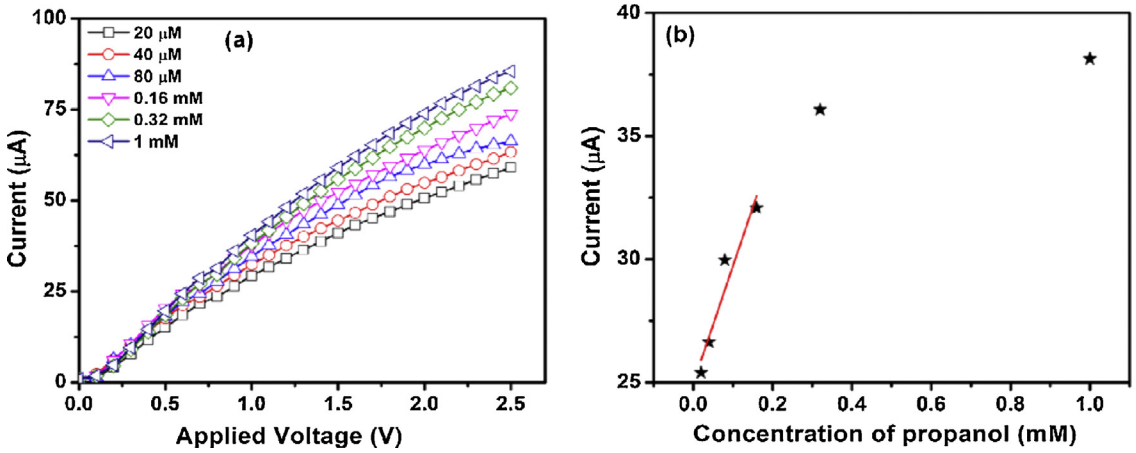

Fig. 10. (a) The *I–V* characteristics of PPy nanobelts based propanol chemical sensor at different propanol concentrations (20 μM–1 mM) in 10 ml of 0.1 M PBS and (b) the calibration curve of current versus methanol concentration of the fabricated chemical sensor.

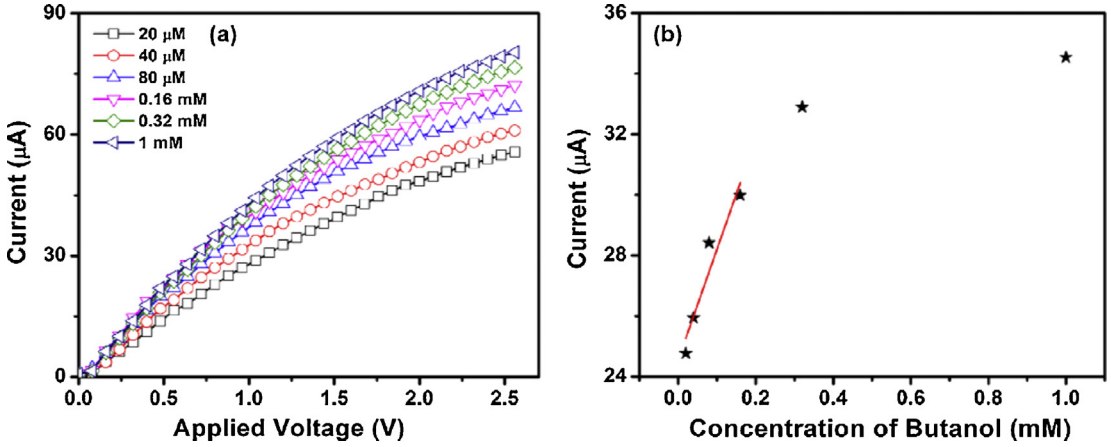

Fig. 11. (a) The *I–V* characteristics of PPy nanobelts based butanol chemical sensor at different butanol concentrations (20 μM–1 mM) in 10 ml of 0.1 M PBS and (b) the calibration curve of current versus methanol concentration of the fabricated chemical sensor.

electrode and forms a weak hydrogen bonding, which is due to the generation of an ion-dipole between -$HN^{+\bullet}$ of PPy and neutral molecule (alcohols) [40]. A hydroxyl terminated PPy is generated by the substitution of adsorbed alcohol on PPy nanobelts electrode [41]. Thus, the terminated hydroxyl might have electrons from the surface of PPy nanobelts to produce the highly reactive oxygenated species, resulting in the decrease of conductance. The releasing of electrons ($\bar{e}$) might significantly dissociate the adsorbed alcohols into CO_2 and H_2O by the electrocatalytic behavior of PPy nanobelts electrode. These electrons are back to the surfaces of PPy nanobelts and again increase the conductance of electrode. In our case, the differences in the sensing response of PPy nanobelts based electrode for different aliphatic alcohols could attribute to the variations in the concentration of adsorbed oxygen species which might considerably affect their sensing reaction and conductance of PPy nanobelts electrode. Additionally, the interference study has been performed to understand the high sensing response of methanol chemical through the fabricated chemical sensor based on PPy nanobelt electrode, as shown in Fig. 12 (c). The methanol, propanol and butanol are consecutively added into PBS to evaluate

Table 1
Sensing response characteristics of various conducting polymers based electrode for different chemicals.

Electrode	Materials	Detection limit	Response time (s)	Correlation coefficient (*R*)	Sensitivity	Refs.
[a]PPy–CFs	Methanol	400 ng	–	–	1.5×10^{-4} (1/μg)	[42]
[a]PPy–CFs	Propanol	2 μg	–	–	3.9×10^{-5} (1/μg)	[42]
[a]PPy–CFs	Hexanol	7.5 μg	–	–	1×10^{-5} (1/μg)	[42]
[b]PAn–PAN/PPO	Phenol	–	–	0.999	960 (μA mM^{-1} cm^{-2})	[43]
[c]GR–PANI/GCE	Phenol	0.065 μM	–	0.9987	177.6; 604.2 (μA mM^{-1})	[44]
Layered PANI sheets electrode	Phenol	4.43 μM	10	0.9981	1485.3 (μA mM^{-1} cm^{-2})	[21]
PPy nanobelts	Methanol	6.92 μM	10	0.98271	205.64 (μA mM^{-1} cm^{-2})	This work
PPy nanobelts	Propanol	13.7 μM	10	0.96401	90.76 (μA.mM^{-1} cm^{-2})	This work
PPy nanobelts	Butanol	12.06 μM	10	0.95931	146.34 (μA mM^{-1} cm^{-2})	This work

[a] PPy–CFs = Polypyrrole–commercial polystyrene fibers electrode
[b] PAn–PAN = Polyaniline–polyacrylonitrile composite electrode.
[c] GR–PANI = Graphene–polyaniline composite electrode.

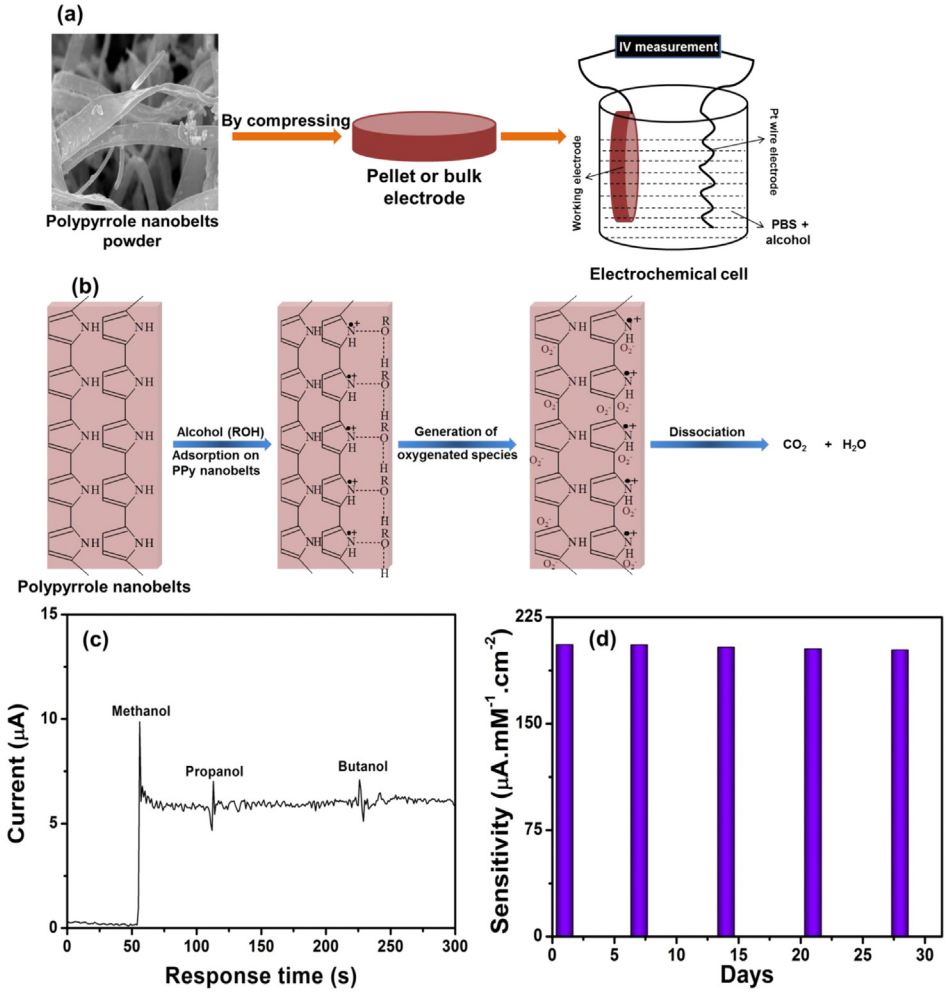

Fig. 12. (a) Schematic illustration of electrochemical system and (b) proposed mechanism of aliphatic alcohol chemical sensors over the surface of PPy nanobelts electrode. (c) Interference tests of the fabricated aliphatic alcohol sensors upon addition of methanol (5 μM), propanol (5 μM), and butanol (5 μM) in PBS (pH 7) and (d) plot of sensitivity versus time interval (days) of the fabricated aliphatic alcohol sensor.

the sensing response. From the amperometic results (Fig. 12(c)), a rapid response current is seen after the addition of methanol while propanol and butanol have shown weak response current. This phenomenon clearly indicates that the fabricated chemical sensor based PPy nanobelt electrode is sensitive to methanol chemical as compared to other aliphatic alcohols.

Fig. 13(A) shows the FTIR spectra of PPy nanobelts electrode before and after the sensing measurements. Before the sensing measurements, the main IR peaks at ~1560 and ~1480 cm^{-1} are observed for PPy nanobelts electrode corresponding to C=C antisymmetric and symmetric stretching vibration in PPy ring respectively [24]. Another main IR peak at ~3206 cm^{-1} presents the N—H stretching in the PPy ring. After the sensing measurements, PPy nanobelts electrode shows almost similar IR spectrum with the peaks of high intensities, indicating that no structural changes have occurred after the sensing measurements. The increase in IR peak's intensity might attribute to the partial interaction between the OH group of alcohols and NH group of PPy nanobelts electrode. Noticeably, no effects or damages have been observed in the structural properties of PPy nanobelts after the sensing measurements in PBS electrolyte with various concentrations of aliphatic alcohols. Therefore, the prepared PPy nanobelts electrode is highly stable in aqueous medium and could be reused for other sensing measurements.

The ^{1}H NMR spectra of PPy nanobelts electrode before and after the sensing measurements as shown in Fig. 13(B), are recorded by 600 MHz FT-NMR spectrometer (JNM-ECA600) in DMSO solvent. The ^{1}H NMR spectra of PPy nanobelt displays the peaks (a, b, c) in the range of 7.0–8.5 ppm, which are assigned to proton of NH group and the aromatic protons on pyrrole ring. After the sensing measurements, two NMR peaks are seen at 5.0–4.5 ppm, indicating the interaction of aliphatic alcohols on PPy nanobelts surface. The NMR peaks at 5.0–4.5 ppm correspond to the protons of carbon, attached with OH group (alcoholic group). The existence of these peaks might suggest that the aliphatic alcohol first interact with the surface of PPy nanobelts through NH group during the sensing measurement, which is proposed in the illustrated mechanism. This result is fully consistent with FTIR results of PPy nanobelts electrode.

The PPy nanobelts electrode based aliphatic alcohols chemical sensor shows the higher sensing performance compared to the reported literatures based on conducting polymers modified electrodes, as shown in Table 1 [21,42–44]. The superior sensitivity and other sensing parameters of PPy nanobelt electrode toward aliphatic alcohol chemical might impute to the excellent adsorption ability and high electrocatalytic/electrochemical activities of PPy nanobelts. Moreover, the fabricated PPy nanobelts electrode based aliphatic alcohol chemical sensor also exhibits good stability and PPy nanobelts electrode retains its sensing performances

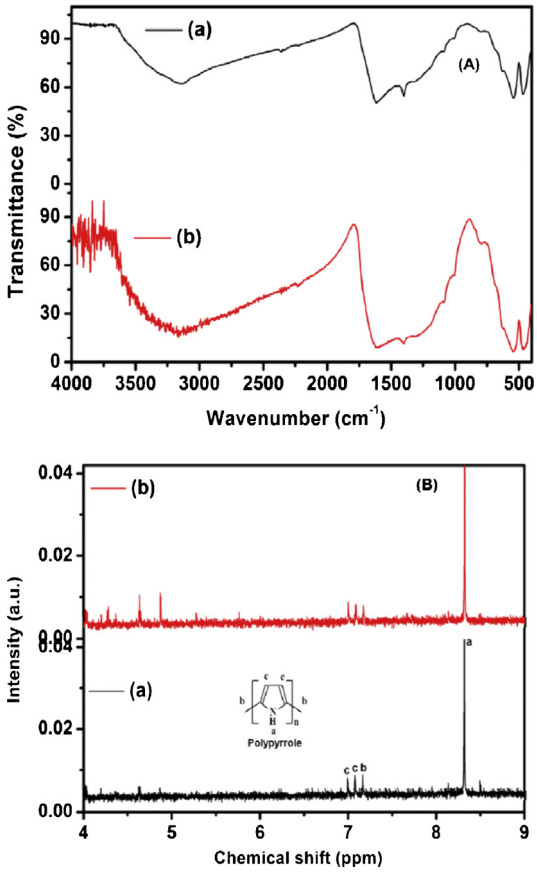

Fig. 13. (A) FTIR and (B) ^{1}H NMR spectra of PPy nanobelts electrode before (a) and after (b) the sensing measurements.

for more than four weeks, as shown in Fig. 12(d). Therefore, PPy nanobelts are the excellent and novel working electrode materials for the fabrication of aliphatic alcohol chemical sensors.

4. Conclusions

The unique PPy nanobelts are simply synthesized by in situ chemical polymerization of pyrrole monomer in the presence of ferric chloride as oxidant and methylene blue as reactive self-degraded template and applied as an effective working electrode for the fabrication of highly sensitive and reproducible aliphatic alcohols chemical sensor. The morphological properties and the elemental mapping demonstrate the uniform morphology of nanobelts and the high aspect of chemical compositions. The PPy nanobelts electrode shows reasonably high electrical conductivity of $\sim 1.80 \times 10^{-4}\ \Omega^{-1}\ cm^{-1}$. The EIS measurements of the fabricated methanol chemical sensor based on PPy nanobelts electrode clearly exhibits low R_{CT} value, indicating the better charge transfer rate and electrocatalytic activity toward the methanol chemical. Whereas, other aliphatic alcohols based chemical sensors are quite inferior to methanol chemical sensor. Furthermore, the current (I)–voltage (V) characteristics have been performed to evaluate the sensing performance of PPy nanobelts electrode toward the detection of aliphatic alcohols. The fabricated PPy nanobelts based electrode shows the rapid detection of methanol with the high sensitivity of $\sim 205.64\ \mu A\ mM^{-1}\ cm^{-2}$, detection limit of $\sim 6.92\ \mu M$ with correlation coefficient (R) of ~ 0.98271 and short response time (10 s).

Acknowledgments

This paper is fully supported by the Research Funds of Chonbuk National University in 2012. This paper was also supported by the Research Funds of Chonbuk National University in 2013 and the NRF Project #2011-0029527 is acknowledged. We would like to thank Mr. Kang Jong-Gyun, Center for University-Wide Research Facilities, Chonbuk National University for his cooperation in TEM images. We also acknowledge the Korea Basic Science Institute, Jeonju branch, for utilizing their research supportive facilities.

References

[1] (a) M. Consales, A. Cutolo, M. Penza, P. Aversa, M. Giordano, A. Cusano, J. Sens. 2008 (2008) 1;
(b) S.C. Kim, W.G. Shim, Appl. Catal. B: Environ. 98 (2010) 180.
[2] P.C. Lekha, M. Balaji, S. Subramanian, D.P. Padiyan, Curr. Appl. Phy. 10 (2010) 457.
[3] P. Pandey, J.K. Srivastava, V.N. Mishra, R. Dwivedi, J. Nat. Gas Chem. 20 (2011) 123.
[4] M.A. Medinsky, D.C. Dorman, Tox. Lett. 82–83 (1995) 707.
[5] E. Segal, R. Tchoudakov, M. Narkis, A. Siegmann, Y. Wei, Sens. Act. B: Chem. 104 (2005) 140.
[6] C.E. Collins, L. Buckley, Synth. Met. 78 (1996) 93.
[7] C.L. Zhu, Y.J. Chen, R.X. Wang, L.J. Wang, M.S. Cao, X.L. Shi, Sens. Act. B: Chem. 140 (2009) 185.
[8] S. Ameen, M.S. Akhtar, H.S. Shin, Talanta 100 (2012) 377.
[9] Y. Lin, H.S. Nalwa, Handbook of Electrochemical Nanotechnology, American Scientific Publishers, USA, 2009.
[10] (a) S. Ameen, M.S. Akhtar, M. Husain, Sci. Adv. Mater. 2 (2010) 441;
(b) R.K. Pandey, V. Lakshminarayanan, Appl. Catal. B: Environ. 125 (2012) 271.
[11] L.A. Mashat, H.D. Tran, W. Wlodarski, R.B. Kaner, K.K. Zadeh, Sens. Act. B: Chem. 134 (2008) 826.
[12] S. Pirsa, N. Alizadeh, Sens. Act. B: Chem. 147 (2010) 461.
[13] (a) S. Pirsa, N. Alizadeh, IEEE J. Sens. 11 (2011) 3400;
(b) R. Aydın, H.Ö. Dogan, F. Köleli, Appl. Catal. B: Environ 140–141 (2013) 478;
(c) W.I. Son, J.M. Hong, B.S. Kim, Korean J. Chem. Eng. 22 (2) (2005) 285.
[14] S.J. Hong, C.H. Lee, Tetrahedron Lett. 53 (2012) 3119.
[15] M. Şenel, C. Nergiz, Curr. Appl. Phy. 12 (2012) 1118.
[16] C.W. Lin, B.J. Hwang, C.R. Lee, Mater. Chem. Phys. 55 (1998) 139.
[17] C.W. Lin, B.J. Hwang, C.R. Lee, J. Appl. Polym. Sci. 73 (1999) 2079.
[18] L. Jiang, H.K. Jun, Y.S. Hoh, J.O. Lim, D.D. Lee, J.S. Huh, Sens. Actuators B 105 (2005) 132.
[19] M. Babaei, N. Alizadeh, Sens. Actuators B Chem. 183 (2013) 617.
[20] F. Quadrifoglio, V. Crescenzi, J. Colloid Interface Sci. 35 (1971) 447.
[21] S. Ameen, M.S. Akhtar, H.S. Shin, Talanta 104 (2013) 219.
[22] S.M. Lin, X. Cao, J.H. Ma, J.J. Wu, H.F. Yin, W.F. Zhu, Dev. Appl. Mater. 2 (2009) 39.
[23] Y. Jia, P. Xiao, H. He, J. Yao, F. Liu, Z. Wang, Y. Li, Appl. Surf. Sci. 258 (2012) 6627.
[24] L.J. Bellamy, The Infrared Spectra of Complex Molecules, 2, 2nd ed., Chapman and Hall, London, 1980.
[25] J.B. Ayers, W.H. Piggs, J. Inorg. Nucl. Chem. 33 (1971) 721.
[26] S. Deivanayaki, V. Ponnuswamy, R. Mariappan, P. Jayamurugan, Optik 1 (2012) Y1KY600K.
[27] G. Han, G. Shi, Sens. Actuators B Chem. 113 (2006) 259.
[28] F.E. Chen, G.Q. Shi, M.X. Fu, L.T. Qu, X.Y. Hong, Synth. Met. 132 (2003) 125.
[29] Y. Fukukawa, S. Tazawa, Y. Fujii, I. Harada, Synth. Met. 24 (1988) 329.
[30] J. Duchet, R. Legras, S. Demoustier-Champagne, Synth. Met. 98 (1988) 113.
[31] A.B. Gongcalves, A.S. Mangrich, A.J.H. Zarbin, Synth. Met. 114 (2000) 119.
[32] M.R. Nabid, A.A. Entezami, J. Appl. Polym. Sci. 94 (2004) 254.
[33] K.G. Neoh, K.K.S. Lau, V.V.T. Wong, E.T. Kang, Chem. Mater. 8 (1996) 167.
[34] A.J.R. Son, H. Lee, B. Moon, Synth. Met. 157 (2007) 597.
[35] P. Fiordiponti, G. Pistoia, Electrochim. Acta 34 (1989) 215.
[36] C.M. Li, C.Q. Sun, W. Chen, L. Pan, Surf. Coat. Technol. 198 (2005) 474.
[37] M.A. Vorotyntsev, J.P. Badiali, G. Inzelt, J. Electroanal. Chem. 472 (1999) 7.
[38] S. Ameen, M.S. Akhtar, G.S. Kim, Y.S. Kim, O.B. Yang, H.S. Shin, J. Alloys Compd. 487 (2009) 382.
[39] P. Feng, Q. Wan, T.H. Wang, Appl. Phys. Lett. 87 (2005) 213111.
[40] M. Hara, A. Eisenberg, Macromolecules 17 (1984) 1335.
[41] L.T. Sein, J. Phys. Chem. A 112 (2008) 598.
[42] S. Pirsa, N. Alizadeh, Sens. Actuators B Chem. 147 (2010) 461.
[43] H. Xue, Z. Shen, Talanta 57 (2002) 289.
[44] Y. Fan, J.H. Liu, C.P. Yang, M. Yu, P. Liu, Sens. Actuators B Chem. 157 (2011) 669.